High-Performance Electrocatalytic PdAuAg Nanoclusters for Ammonia Oxidation

Stephen Nzioki Mailu*

Department of Physical Sciences, Machakos University, P.O. Box 136-90100, Machakos, Kenya.
Corresponding Author: Stephen Nzioki Mailu

Abstract: *Catalytic oxidation of ammonia provides a promising technique for the generation of hydrogen. In this work, the electro-oxidation of ammonia on palladium-gold-silver ternary nanoclusters (PdAuAgNPs) on platinum (Pt) electrode was systematically studied in alkaline solution of potassium hydroxide (KOH) by cyclic voltammetry. The PdAuAg nanoclusters were prepared through a facile synthesis with ascorbic acid as a reductant and poly(vinyl pyrrolidone) (PVP) as a stabilizing agent from aqueous solutions of $PdCl_2/HAuCl_4.3H_2O/AgNO_3$ mixtures. High resolution transmission electron microscopy (HRTEM) revealed the formation of crystalline non-aggregated 25-35 nm sized nanoalloys. The electrocatalytic behaviour of the PdAuAg nanoclusters for ammonia oxidation showed reduced overpotential properties and an increased current density compared to the bare Pt electrode thus providing a promising route for development of low-cost and high-performance electrocatalyst for electro-oxidation of ammonia.*
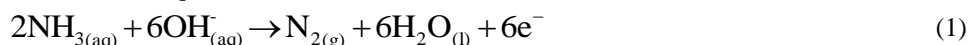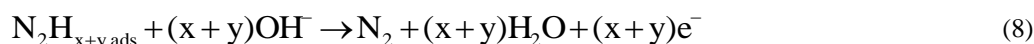***Keywords****: Electrocatalyst; nanoalloys; ammonia oxidation; nanoclusters; hydrogen*

I.   Introduction

The use of hydrogen as a source of fuel for fuel cells as well as the emergence of legislation promoting hydrogen economy has made production of hydrogen a very important topic in chemistry and engineering. However, its storage and transportation is both inefficient and dangerous [1]. Discovering a feasible hydrogen production process is very important to the future of energy production. Liquid ammonia has been identified as a suitable hydrogen carrier and is one of the highly-used commodity chemicals in the world; its storage, transportation, and handling procedures are well-known and documented [2]. Liquid ammonia contains 1.7 times more hydrogen than liquid hydrogen. It is easy to handle under low pressure and boasts a specific energy density 50% higher than liquid hydrogen for a given volume [3]. Ammonia is also easily condensed at ambient temperatures and pressure which makes it a good choice for transportation and storage. Its decomposition by electro-oxidation in alkaline media at low overpotentials is NO_x and CO_x free with nitrogen and water as products of the reaction [4]. Therefore, ammonia offers a significant advantage in cost and convenience over pure hydrogen as an alternative fuel for clean energy supply. The ammonia electro-oxidation reaction can be coupled with the hydrogen evolution reaction for the production of high-purity hydrogen in an alkaline electrocatalytic cell. It is oxidised at the anode (equation 1) at a potential of 0.77 V (vs. standard hydrogen electrode, SHE). Alkaline reduction of water occurs at the cathode (equation 2) and requires -0.83 V vs. SHE. Overall (equation 3), 0.06 V is required [5];

$$2NH_{3(aq)} + 6OH^-_{(aq)} \rightarrow N_{2(g)} + 6H_2O_{(l)} + 6e^- \tag{1}$$

$$6H_2O_{(l)} + 6e^- \rightarrow 3H_{2(g)} + 6OH^-_{(aq)} \tag{2}$$

$$2NH_{3(aq)} \rightarrow N_{2(g)} + 3H_{2(g)} \tag{3}$$

The thermodynamic values thus favour the production of hydrogen coupled to the ammonia oxidation compared to hydrogen production by electrolysis of water, whose theoretical cell voltage is 1.223 V [6]. The aqueous high capacity for hydrogen storage has led to increased interest in using ammonia as an alternative energy carrier. Extracting this hydrogen from ammonia can be accomplished through the use of electrochemical approaches. The development of electrocatalytic techniques for ammonia oxidation has attracted much attention as alternative energy supply with platinum being the commonly used electrocatalytic material. Gerischer and Mauerer [7] proposed the mechanism of ammonia oxidation on platinum:

$$NH_{3(aq)} \rightarrow NH_{3,ads} \tag{4}$$

$$NH_{3,ads} + OH^- \rightarrow NH_{2,ads} + H_2O + e^- \tag{5}$$

$$NH_{2,ads} + OH^- \rightarrow NH_{ads} + H_2O + e^- \tag{6}$$

$$NH_{x,ads} + NH_{y\,ads} \rightarrow N_2H_{x+y,ads} \tag{7}$$

$$N_2H_{x+y\,ads} + (x+y)OH^- \rightarrow N_2 + (x+y)H_2O + (x+y)e^- \tag{8}$$

$$NH_{ads} + OH^- \rightarrow N_{ads} + H_2O + e^- \tag{9}$$

Where x = 1 or 2, y = 1 or 2.

According to this mechanism, the partially dehydrogenated species of NH_{ads} and $NH_{2,ads}$ are the active intermediates to form the final product of N_2 in equation 8, whereas N_{ads} formed in equation 9 tends to block the electrode surface and become a poison [8]. Vooys *et al*., [9] discussed the correlation between the electrocatalytic activity of ammonia oxidation and the adsorption energy of N_{ads} on various metals such as Ru, Rh, Pd, Ir, Pt, Au, Ag and Cu. Their N_{ads} adsorption energies were found to follow the trend (decreasing N_{ads} activity); Ru > Rh > Pd > Ir > Pt >> Au, Ag and Cu. Pt is the best electrocatalyst because metals having smaller N_{ads} adsorption energy than Pt (e.g. Cu, Ag and Au) are inactive in equation 5 or 6 and is almost insensitive to the poisoning among the platinum group metals. However, alloying platinum group metals (PGMs) with other noble metals is believed to increase the electrocatalytic activity for ammonia oxidation in alkaline solutions. Endo *et al*., [8] pointed out that alloying Pt and Ir leads to enhanced electrocatalytic activity for ammonia oxidation in alkaline solutions. Pd which has the same d-valence electrons as Pt, less expensive than Pt and one of the platinum group metals is also a promising electrocatalyst based on its electroactivity towards ammonia. However, it has a high N_{ads} making its application as an electrocatalyst a major challenge. It is believed that alloying it with noble metals having smaller N_{ads} adsorption energy such as Cu, Au and Ag will lower its high N_{ads} adsorption and increase its catalytic properties towards ammonia oxidation.

To the best of our knowledge, there is no literature report on the synthesis of PdAuAg ternary nanoalloy and its subsequent application in the oxidation of ammonia. In the present study, PdAuAg ternary alloy system has been chemically synthesised by the use of ascorbic acid as the reducing agent and poly(vinyl pyrrolidone) (PVP) as the capping agent and investigated towards the oxidation of ammonia.

II. Experimental Methods
2.1 Reagents and Materials
Palladium chloride ($PdCl_2$), Hydrogen tetrachloroaurate (III) trihydrate ($HAuCl_4.3H_2O$) (99.99%), Silver nitrate ($AgNO_3$), ascorbic acid, poly(vinyl pyrrolidone) (PVP, MW = 55000), ammonium hydroxide (NH_4OH), lithium perchloride ($LiClO_4$) and potassium hydroxide (KOH) were all purchased from Sigma-Aldrich. Alumina micro powder and polishing pads were obtained from Buehler, IL, USA and were used for polishing the Pt electrodes. Ultra-pure water (Millipore) was used in the preparation of the aqueous solutions.

2.2 Measurements and Instrumentations
All voltammetric measurements were performed on a BAS 100W electrochemical workstation from BioAnalytical Systems Incorporation (Lafayette, USA) using a three-electrode cell system consisting of Pt electrode (1.6 mm diameter), Ag/AgCl (saturated NaCl) and platinum wire as working, reference and counter electrodes, respectively. All experimental solutions were purged with high purity argon gas and blanketed with the same during measurements. The experiments were carried out at controlled room temperature (25 ºC). UV-vis spectra measurements were recorded with the Nicolette Evolution 100 Spectrometer (Thermo Electron Corporation, UK). High resolution transmission electron microscopy (HRTEM) images were acquired using a Tecnai G^2 F_2O X-Twin MAT. The HRTEM characterizations were performed by placing a drop of the solution on a carbon coated copper grid and dried under electric bulb for 30 min. Surface morphology of the nanoalloys were studied by atomic force spectroscopy (AFM) using a Veeco NanoMan V model. The AFM experiments were performed with a silicon tip at a spring constant of 1-5 N/m and resonance frequency of 60-100 kHz. For the catalytic oxidation of ammonia, the electrochemical measurements were performed at 25 ºC in 0.1 M ammonia and 1 M KOH aqueous solution saturated with argon gas. Cyclic voltammetric measurements were performed in the presence and absence of ammonia at the sweep rates of 10-100 mV s^{-1} between -1000 mV and 100 mV.

2.2 Preparation of the PdAuAg ternary nanoclusters
In a typical synthesis of PdAuAg ternary nanoclusters, 1.5 mL of a 5 mM aqueous solution of $PdCl_2/HAuCl_4/AgNO_3$ mixtures was added to 45.5 mL of highly purified water. To this solution, 1.5 mL of 0.1 M ascorbic acid was added. After 15 s, an aqueous solution of PVP (5 mg/mL, 1.5 mL) was added drop wise with vigorous stirring, and the solution was stirred further for 30 min. The resulting hydrosol was subjected to centrifugation to remove excess PVP. Pd, PdAu and PdAg nanoparticles were prepared in the same way by

substituting aqueous solutions of PdCl$_2$/HAuCl$_4$/AgNO$_3$ mixtures by PdCl$_2$, PdCl$_2$/HAuCl$_4$ and PdCl$_2$/AgNO$_3$ solutions, respectively.

### 2.3 Fabrication of PdAuAg nanoclusters modified Pt electrode

Prior to modification, the bare Pt electrode was polished to a mirror finish with 1.0, 0.3, and 0.05 μm alumina slurries, respectively, and then rinsed thoroughly with distilled water followed by sonication in ethanol and water, respectively. 10 μL solutions of already synthesised PdAuAg nanoclusters were drop-coated on the Pt electrode and allowed to dry at room temperature. The modified electrode was taken out and rinsed with water carefully, and henceforth denoted as Pt|PdAuAgNPs. Pd, PdAu and PdAg-modified Pt electrodes were as well prepared by drop-evaporation over the bare Pt electrode, and each henceforth denoted as Pt|PdNPs, Pt|PdAuNPs and Pt|PdAgNPs, respectively.

III.   Results and Discussions
3.1 Spectroscopic and microscopic characteristics of PdAuAg ternary nanoclusters
3.1.1 UV-Visible spectroscopy

The formation of the nanoparticles by reduction of Pd^{2+}, HAuCl$_4^-$ and Ag$^+$ ions was confirmed by the use of UV-visible spectroscopy. Fig. 1 shows the UV-visible spectra of PdCl$_2$, AgNO$_3$ and HAuCl$_4$.3H$_2$O solutions while Fig. 1-inset shows the UV-visible spectra of Pd, PdAu, PdAg, and PdAuAg nanoparticles. The absorption peaks observed at 260 nm for AgNO$_3$, 285 nm for HAuCl$_4$.3H$_2$O and 420 nm for PdCl$_2$ (attributed to the existence of Pd(II)) [10] disappeared after the reduction indicating that the Ag$^+$, HAuCl$_4^-$ and Pb^{2+} ions were completely reduced. The synthesized nanoparticles showed no absorption peaks indicating a complete reduction of the metal salts and the colour of the solution turned from pale yellow to black.
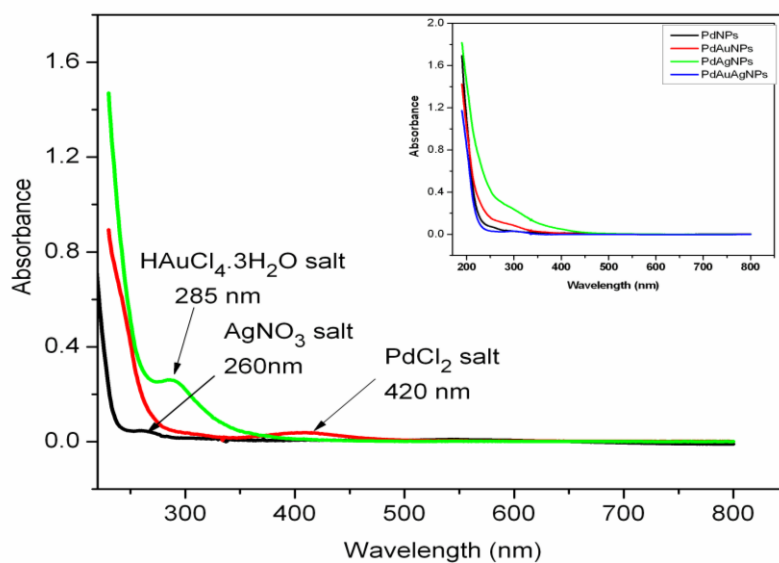

Figure 1. UV-vis spectra of PdCl$_2$, AgNO$_3$ and HAuCl$_4$.3H$_2$O solutions (Inset: UV-vis spectra of Pd, PdAg, PdAu and PdAgAu nanoclusters)

3.1.2 High resolution transmission electron microscopy

The size, shape and the crystalline properties of the nanoparticles were investigated using high resolution transmission microscopy (HRTEM). Fig. 2A shows typical HRTEM image of the prepared Pd nanoparticles. The nanoparticles produced were found to be well dispersed with an average diameter of 40-50 nm. HRTEM image of a single particle (not shown) revealed atomic lattice fringes demonstrating the crystalline nature of the nanoparticles. PdAg polycrystalline 5-12 nm sized bimetallic nanoparticles were obtained whose crystalline nature was evidenced by the presence of the lattice fringes (Fig. 2B). Non-aggregated 20-30 nm sized PdAu bimetallic nanoclusters synthesized using the same procedure were observed as shown in Fig. 2C. The non-aggregation of the nanoclusters is believed to have resulted from the electrostatic partial negatively charged oxygen atom present in the amide group of the PVP. The observed images are similar to those reported in literature for PdAu bimetallic nanoparticles [11]. For the PdAuAg ternary alloy nanoclusters, crystalline non-aggregated 25-35 nm sized nanoclusters were formed (Fig. 2D). Although the formation mechanism of PdAuAg alloy nanoclusters is not clear, it can be assumed that unstable small nanoparticles aggregate into the three-dimensional nanoclusters (flower-shaped nanoparticles). Close inspection of the HRTEM images shows that the nanoclusters are built up by sixes of elongated primary nanoparticles with average dimensions of approximately

10 nm, and boundaries and voids between the components are present (see inset of Fig. 2D). The formation of nanoclusters with flower-shaped porous structures or multi-branched structures has also been reported in literature. Lee *et al.,* [12] reported the synthesis of flower-shaped Au-Pd alloy nanoparticles. Teng *at al.,* [13] proposed a 'self-organization' mechanism for the fabrication of porous Pt nanoparticles. Flower-shaped Rh nanoparticles were also reported by Hoefelmeyer and co-workers [14]. It was found that ascorbic acid might promote the formation of multipodal or porous particles [15-16]. However, the ascorbic reduction mechanism cannot explain the formation of the synthesized flower-shaped porous PdAuAg ternary nanoclusters entirely, because we could not obtain flower-shaped monometallic Pd and bimetallic PdAg nanoparticles under the same experimental conditions.
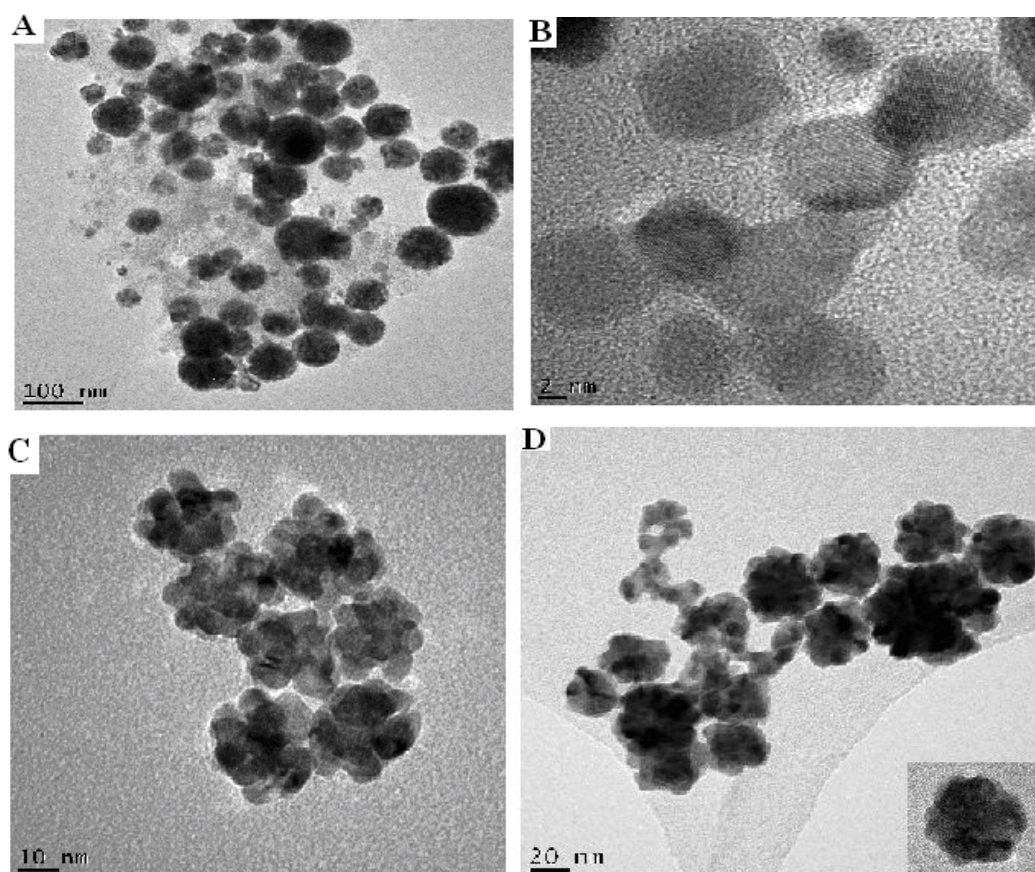
Figure 2. HRTEM images of Pd nanoparticles (A), PdAg nanoparticles (B), PdAu nanoclusters (C) and PdAuAg nanoclusters (D).

3.1.3 Atomic Force Microscopy Analysis

Atomic force microscopy (AFM) has become a standard technique for high resolution imaging of the morphology and topography of surfaces. It operates by measuring the force between the probe and the sample. The interaction of the force fields is sensed by a cantilever beam, to which the tip is attached. An image (revealing individual atoms) is created as the probe is translated across the surface [17]. AFM analyses were carried out for PdNPs, PdAgNPs, PdAuNPs and PdAuAgNPs in order to investigate the differences in their surface morphology and topography. Fig. 3 shows the AFM images of the silicon substrate used and the substrate modified with different nanomaterials; PdNPs, PdAgNPs, PdAuNPs and PdAuAgNPs. As can be seen from Fig. 3B, a random distribution of Pd nanoparticles over the silicon substrate was observed. The sizes of the formed Pd nanoparticles were found to be below 100 nm, which correlated well with the HRTEM results. PdAgNPs and PdAuNPs (Fig. 3C and D) showed well distributed nanoparticles on the substrate indicating the polycrystalline nature of the nanoparticles correlating well with the HRTEM images. The most interesting thing is the fact that round beaded patchy shaped surface of the PdAuAgNPs (Fig. 3E) was observed which corroborated the HRTEM images (nanoclusters).
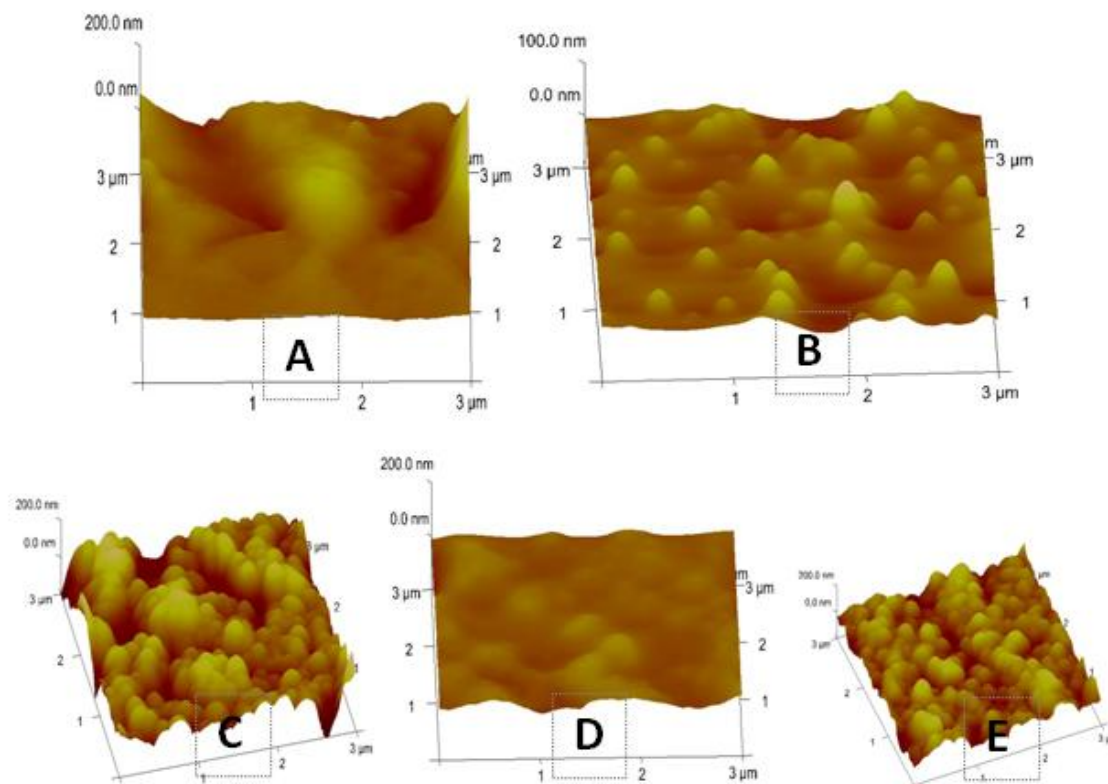
Figure 3. AFM images of silicon substrate (A), Pd nanoparticles (B), PdAg nanoparticles (C), PdAu nanoparticles (D) and PdAuAg nanoclusters (E).

## 3.2 Electrochemistry of $PdCl_2$, $AgNO_3$ and $HAuCl_4.3H_2O$ solutions

The redox reactions of $PdCl_2$, $AgNO_3$ and $HAuCl_4.3H_2O$ solutions on Pt electrode were investigated by cyclic voltammetry (CV) in 0.1 M $LiClO_4$ Ar-saturated solution. The CVs were recorded over a potential range of -500 mV and 1000 mV at a scan rate of 100 mV s^{-1}. For the $PdCl_2$ solution, three oxidation peaks were observed; peak a, $E_{p,a}$ = -300 mV followed at more positive potentials by peaks b, $E_{p,a}$ = -158 mV and c, $E_{p,a}$ = 717 mV. On the cathodic scan, two reduction peaks were also observed c′, $E_{p,c}$ = 284 mV, and b′, $E_{p,c}$ = -253 mV (Fig. 4a). However, to ascertain whether there was a cathodic peak that was related to peak a, a wider potential range of -700 mV to 1000 mV was used and a third cathodic peak, a′, $E_{p,c}$ = -467 mV (Fig. 4a-inset) was observed. The observed peaks can be related to the different possible palladium oxidation states such as Pd(0), Pd(II), and Pd(IV) that may undergo several redox reactions such as Pd(0) nanoparticles deposit or Pd(0) oxidation to Pd(II) and Pd(IV) [18]. Redox peaks a/a′ and b/b′ are due to the oxidation and reduction of adsorbed and absorbed hydrogen, respectively. At positive potentials, Pd^0 nanoparticles deposited on the Pt surface during the cathodic scanning are oxidized to Pd^{2+} ($Pd^0 \rightarrow Pd^{2+} + 2e^-$) (peak c) and form a palladium oxide layer. The Pd oxide is reduced on the negative-going scans to Pd metal ($Pd^{2+} + 2e^- \rightarrow Pd^0$) (peak c′). It is noteworthy that Pd oxide layer reduction may occur in a reversible or irreversible manner depending on the upper switching potential. Based on the results obtained, the reduction of the palladium oxide layer behaved in an irreversible manner ($I_{p,a}/I_{p,c} \neq 1$ and $\Delta E_p > 59$ mV) which can be explained by the formation of both PdO and PbO_2 [18]. Interrogating $AgNO_3$ using CV showed a pair of redox peaks with anodic peak potential ($E_{p,a}$) of 211 mV and cathodic peak potential ($E_{p,c}$) of +11 mV for Ag^+/Ag^0 process [19] as shown in Fig. 4b. The CV of $HAuCl_4.3H_2O$ solution showed one reduction peak at 704 mV, which corresponds to the reduction of solution bound Au(III) to Au(0) [20]. A reduction peak appears at 930 mV which can be attributed to the reduction of adsorbed $AuCl_4^-$. No anodic peak for Au(0) was observed on the reverse scan indicating the irreversibility of the reduction of Au(III) [20] (Fig. 4c).
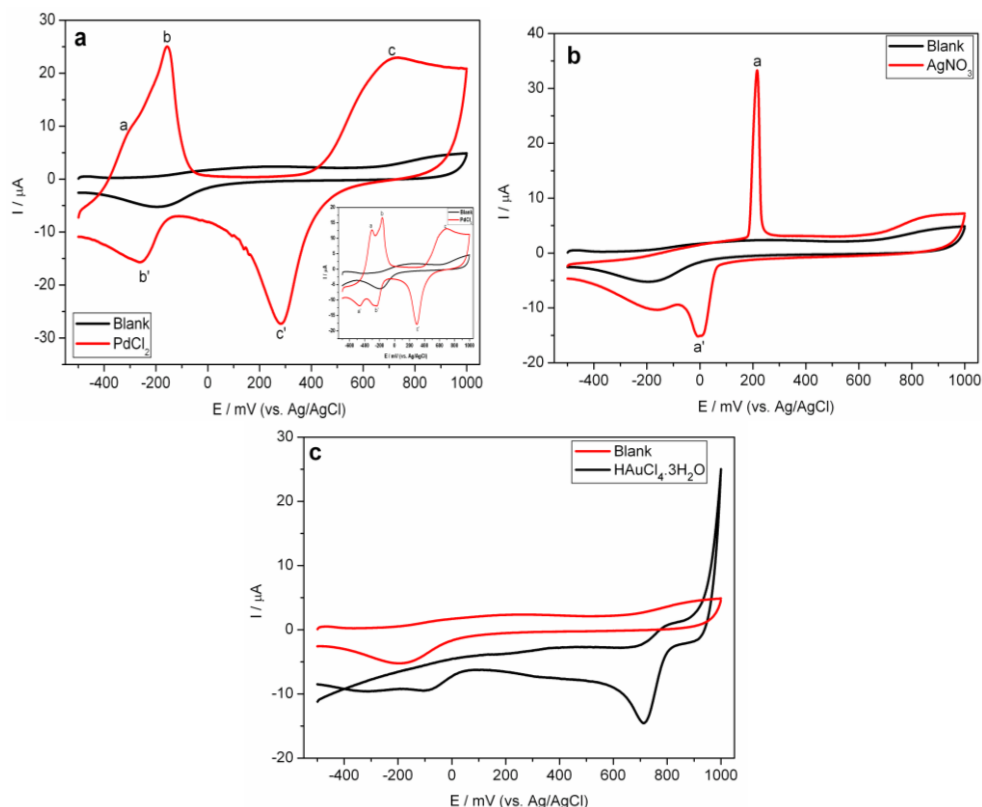
Figure 4. CVs of 5 mM $PdCl_2$ solution (a) 5 mM $AgNO_3$ solution (b) and 5 mM $HAuCl_4.3H_2O$ solution (c) in 0.1 M $LiClO_4$ at a scan rate of 100 mV s^{-1}.

**3.3 Electrochemical characteristics of PdAuAg ternary nanoclusters**

The characterization of the surface of nanoparticles is a very important issue in the applications of nanoparticles as catalysts and sensors. For instance, catalytic effects are influenced strongly by the structure and composition of the surface of nanoparticles. PdAuAg nanoclusters were characterized by CV measurements which is a useful technique for interrogating the electrochemical behaviour of nanomaterials. Fig. 5 shows a series of cyclic voltammograms of the bare Pt electrode and those of the Pt electrode modified with the synthesized nanoparticles. These were recorded in 0.1 M $LiClO_4$ at a scan rate of 100 mV s^{-1} in the potential range of -500 mV to 1000 mV. The bare Pt electrode showed typical potential ranges for the hydrogen adsorption/desorption (-500 mV to -100 mV), double layer potential range (100 mV to -550 mV Ag/AgCl and the formation/reduction of the surface Pt oxide, Pt-OH$_{ads}$ (550 to –1000 mV)(Ag/AgCl) as described by Zhong *et al*., [3]. For the Pd nanoparticles modified Pt electrode (Pt|PdNPs), the appearance of an anodic peak (Fig 5A, peak a, $E_{p,A}$ = -200 mV) and a cathodic peak (Fig. 5A, peak a′, $E_{p,c}$ = -110 mV) is attributed to the desorption and adsorption of hydrogen atoms onto the Pd^0 nanoparticles, respectively as shown in scheme 1 [21]. The Pd^0 nanoparticles on the Pt electrode surface were oxidized to Pd^{2+} and formed a palladium oxide layer (Fig. 5A, peak b, $E_{p,a}$ = 650 mV) . On the cathodic CV scan, a reduction peak (Fig. 5A, peak b′, $E_{p,c}$ = 310 mV) occurred corresponding to the reduction of the Pd oxide layer. Lee *et al*., [22] observed similar peaks on Pd nanoparticles modified ITO electrodes.
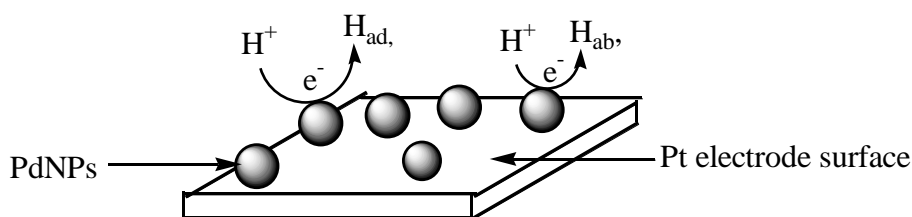
Scheme 1. Schematic representation of the surface of Pt electrode with Pd nanoparticles. The proton reduction takes place on the surface of the Pd nanoparticles

PdAu nanoalloys modified Pt electrode (Pt|PdAuNPs)(Fig. 5B) showed current peaks of hydrogen desorption/adsorption at low potentials (peak a, $E_{p,a}$ = -245 mV and peak a′, $E_{p,c}$ = -290 mV) and surface

oxidation/reduction at high potentials (peak b, $E_{p,a}$ = 454 mV and peak b′, $E_{p,c}$ = 363 mV) which revealed a typical CV characteristics of a 'palladium-like' modified electrode. However, the reduction peak of surface oxide showed an anodic shift on the PdAu nanoalloys compared to that of Pd nanoparticles (310 mV to 363 mV) indicating an easier removal of adsorbed oxygen species from PdAu nanoalloys compared to that from Pd monometallic nanoparticles [23]. The CV of PdAg nanoalloys modified electrode (denoted as Pt|PdAgNPs) (Fig. 5C) showed hydrogen desorption/adsorption at low potentials (peak a, $E_{p,a}$ = -180 mV and peak a′, $E_{p,c}$ = -215 mV, respectively) and surface oxidation/reduction at high potentials (peak c, $E_{p,a}$ = 788 mV and peak c′, $E_{p,c}$ = 291 mV). A redox peak was observed, b/b′ (peak b, $E_{p,a}$ = 250 mV and peak b′, $E_{p,c}$ = 35 mV) which was attributed to the Ag/Ag$^+$ redox system (refer to Fig. 4). For the PdAuAg nanoalloys modified electrode (Pt|PdAuAgNPs) (Fig. 5D), hydrogen desorption/adsorption peaks (peak a, $E_{p,a}$ = -220 mV and peak a′, $E_{p,c}$ = -270 mV) and surface oxidation/reduction peaks (peak c, $E_{p,a}$ = 810 mV and peak c′, $E_{p,c}$ = 350 mV) were observed. A redox peak was observed (peak b, $E_{p,a}$ = 240 mV and peak b′, $E_{p,c}$ = 55 mV) which can be attributed to the Ag/Ag$^+$ redox system. It is noteworthy that the reduction peak of surface oxide showed an anodic shift and the hydrogen desorption/adsorption peak currents for the Pt|PdAuAgNPs decreased compared to that observed for Pt|PdAgNPs which can be attributed to the total incorporation of the Au in the nanoalloys system. Considering the reduction potentials of Au^{3+} (AuCl$_4^-$/Au, +1.002 V vs. SHE), Pd^{2+} (Pd^{2+}/Pd, +0.591 V vs. SHE) and Ag$^+$ (Ag$^+$/Ag, +0.80 V vs. SHE), it can be assumed that the formation of the nanoalloys was initiated by nucleation of Au atoms followed by co-deposition/incorporation of residual Au, Ag and Pd atoms on the surface of the seeds which have higher Au content [22]. These results correlated well with the electrochemical behaviour of the metal precursor solutions studied in Fig. 4.
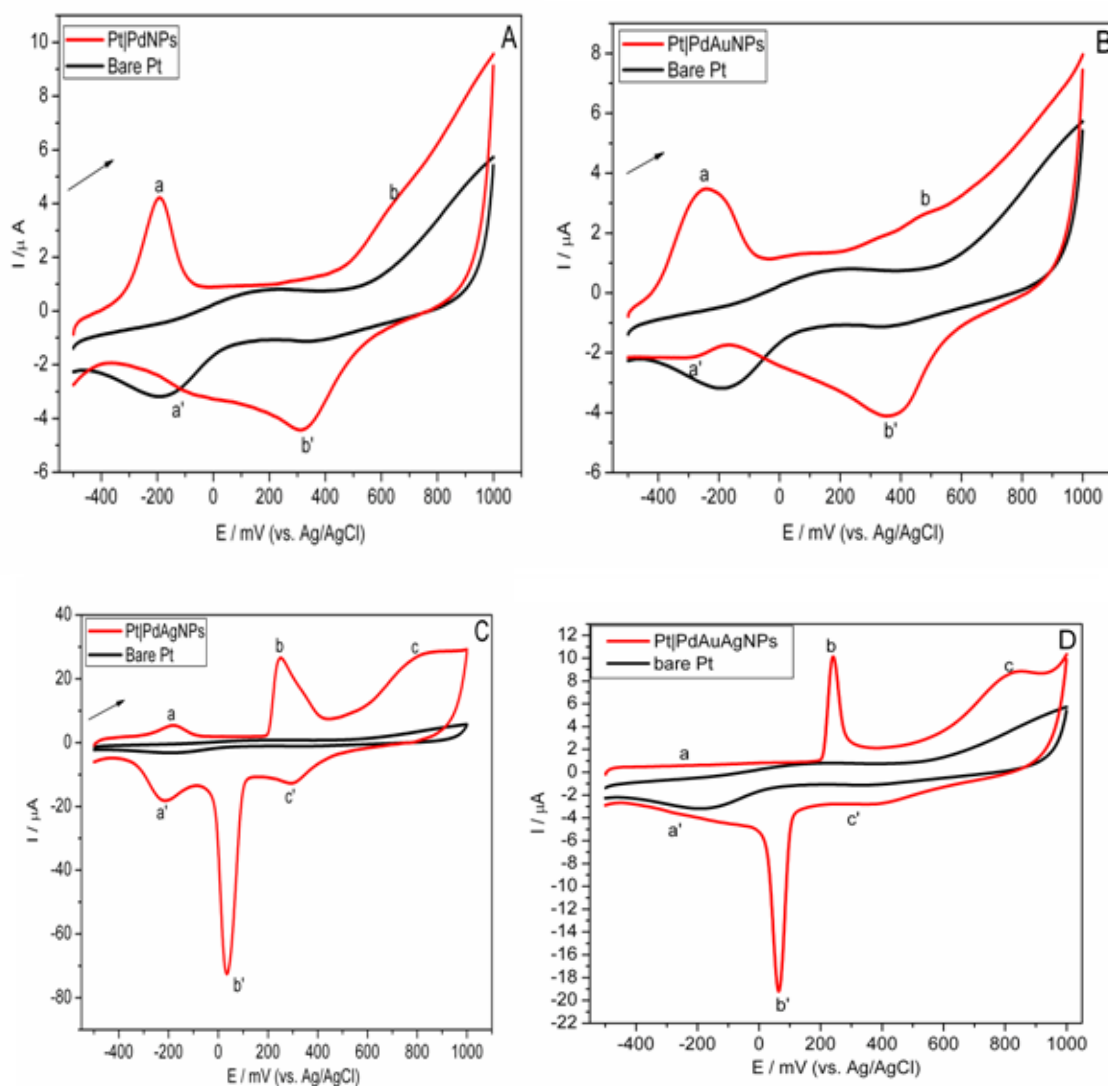

Figure 5. Cyclic voltammograms of Pt|PdNPs (A), Pt|PdAuNPs (B), Pt|PdAgNPs (C) and Pt|PdAuAgNPs (D) in 0.1 M LiClO$_4$ at a scan rate of 100 mV s^{-1}.

3.4 The catalytic performance of PdAuAg alloy nanoclusters
3.4.1 Catalytic oxidation of ammonia

Fig. 6 shows the cyclic voltammograms of Pd, PdAg, PdAu and PdAuAg nanoalloys modified Pt electrodes in 1 M KOH aqueous solution with and without 0.1 M ammonia. The anodic peak at -950 mV was attributed to the oxidation of hydrogen while that at -292 mV (Ag/AgCl) was assigned to the oxidation of ammonia to N_2 [24]. Two reduction peaks appear at −500 mV and −839 mV. The cathodic peak at −500 mV is related to the reduction/desorption of oxidized species of ammonia such as NH_{ads} and $NH_{2,ads}$ while that observed −839 mV corresponds to the reduction of oxidized species such as nitrite anions [8]. It is no doubt that ammonia oxidation (between -400 mV and -250 mV) proceeds on all of these electrodes, although both the potential and the peak currents of the oxidation peaks are dependent on the electrode material. When the Pt electrode was coated with PdNPs, there was current increase and lower overpotential compared to the bare electrode while PdAg and PdAu alloys modified Pt electrode showed a decreased peak current and higher overpotential. Since the ammonia concentration was kept constant for all the experiments, the decreased peak currents on PdAgNPs and PdAuNPs modified Pt electrodes may suggest that the active sites are less dense than on bare Pt electrode. Vooys *et al*., [9] highlighted that Cu, Ag and Au are inactive towards ammonia oxidation. Although the PdAg and PdAu alloys were expected to have a higher catalytic effect than the monometallic PdNPs, the inactiveness of Ag and Au in the alloy may have lowered the catalytic ammonia oxidation activity of the alloy. PdNPs increased the surface area of the Pt electrode thus increasing the peak current compared to the bare Pt electrode. It is believed that the surface orientation of the electrodes used in ammonia oxidation determine their catalytic properties. A recent report [25] revealed that the catalytic activity of ammonia on Pt single crystals is highest on (100) plane. Since the orientation on the surface of the electrode used in this study was the same, the density of the active site could be assumed to be dependent on the constituents of the electrode material. Though the surface active sites of the Pt electrode are expected to become less available when coated with nanoparticles, PdAuAg nanoclusters were found to give slightly higher peak currents and lower overpotential than bare Pt (see Table 1), which can be explained by cooperative effects between Pd and the noble metals, Au and Ag. This showed that PdAuAg nanoclusters were suitable electrocatalysts for ammonia oxidation based on their reduced overpotential and increased current properties.
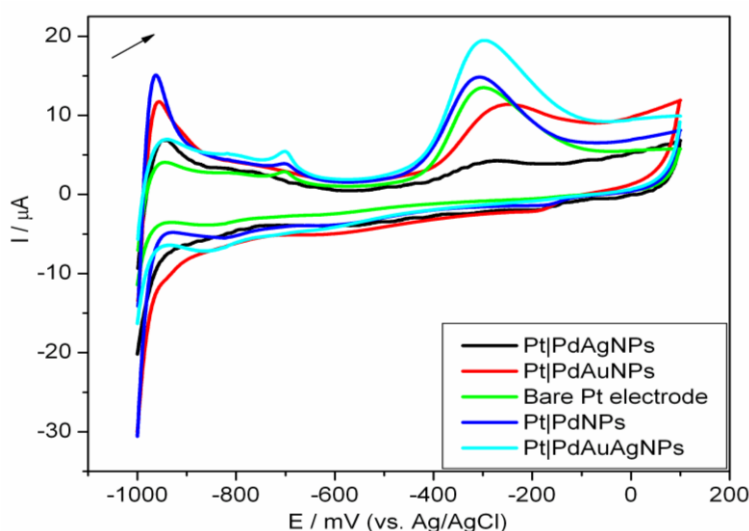
Figure 6. CVs of Pt, Pt|PdNPs, Pt|PdAgNPs, Pt|PdAuNPs and Pt|PdAuAgNPs in 0.1 M ammonia and 1 M KOH aqueous solution at a scan rate of 50 mVs^{-1}.

**Table 1.** Data extracted from **Figure 6.**

Electrode	$E_{p,a}$ (mV)	$I_{p,a}$ (A)
Pt electrode	-300	1.371×10^{-5}
Pt|PdNPs	-311	1.521×10^{-5}
Pt|PdAuNPs	-255	1.145×10^{-5}
Pt|PdAgNPs	-282	4.380×10^{-6}
Pt|PdAuAgNPs	-304	1.992×10^{-5}

3.4.2 Effects of ammonia concentration

Fig. 7 shows the cyclic voltammograms measured on Pt|PdAuAgNPs in 1 M KOH solution with various ammonia concentrations. It can be seen that two anodic current peaks were observed at approximately -940 mV and -292 V (Ag/AgCl) in all the curves, respectively. With the increase in ammonia concentration, the

peak current at -292 mV increased continuously. This can be attributed to the adsorption of more ammonia on the electrode surface which has to be oxidized. Thus, the anodic current increases continuously with the ammonia concentration. In particular, there was a significant increase in peak current when the ammonia concentration increased from 0.05 M to 1 M. When the ammonia concentration reached a certain content, i.e. 1 M the adsorption of ammonia on Pt|PdAuAgNPs electrode achieved a relatively saturation status. The further increase of the ammonia concentration in the solution apparently enhanced the amount of ammonia to be oxidized. However, the intermediates generated during ammonia oxidation, such as $NH_{2,ads}$ and NH_{ads}, could remain on the electrode surface and block the ammonia adsorption. It is reasonable to assume that the blocking effect will be significant when the solution contains a high concentration of ammonia. Therefore, an increase of the ammonia concentration beyond 1 M resulted in slight decrease in anodic peak current due to ammonia saturation on the electrode surface. The present results show that ammonia can be oxidised effectively on Pt|PdAuAgNPs electrode.
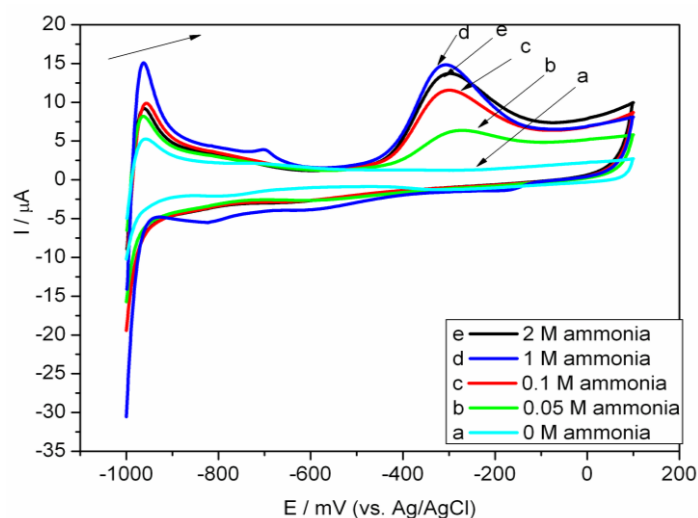
Figure 7. Cyclic voltammograms measured on Pt|PdAuAgNPs in 1 M KOH solutions with the various concentrations of ammonia (0.05-2 M ammonia).

3.4.3 Effects of potential scanning rate

In order to study the nature of the oxidation of ammonia, CVs at different scan rates measured on Pt|PdAuAgNPs in 0.1 M ammonia and 1 M KOH solution were performed (Fig. 8). The anodic peak currents at about -292 mV increased significantly with the increasing potential scan rate. The peak currents followed a linear $v^{1/2}$ (v: potential scan rate) dependence indicating a diffusion controlled rather than a surface controlled electron transfer kinetics. Additionally, the peak potential changed positively with increasing scan rates, demonstrating that the oxidation of ammonia was an irreversible process [26].
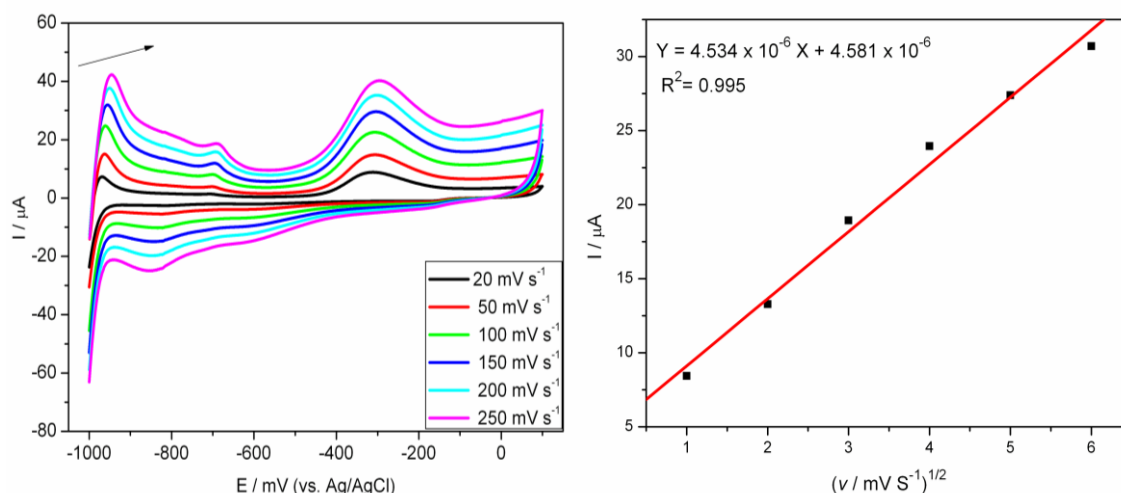
Figure 8. CV of Pt|PdAuAgNPs in the presence of 0.1 M ammonia and 1 M KOH aqueous solution at different scan rates and a plot of peak currents as a function of the square root of potential scan rate.

For an irreversible diffusion-controlled process, the peak potential (E_p) is proportional to the logarithm of potential sweep rate (v) within the following equation [21, 27]:

$$E_p = \frac{b}{2}\log v + \text{constant} \qquad (10)$$

On the basis of this equation, the plot of E_p versus log v linear plot is b/2, where b indicates the Tafel plot whose value was calculated to be about 30 mV per decade (Fig. 9). This value is reasonably close to the theoretical value of 40 mV decade, typical for an electrochemical reaction involving at least two electron-transfer steps, the second electron transfer being the rate determining step [28].
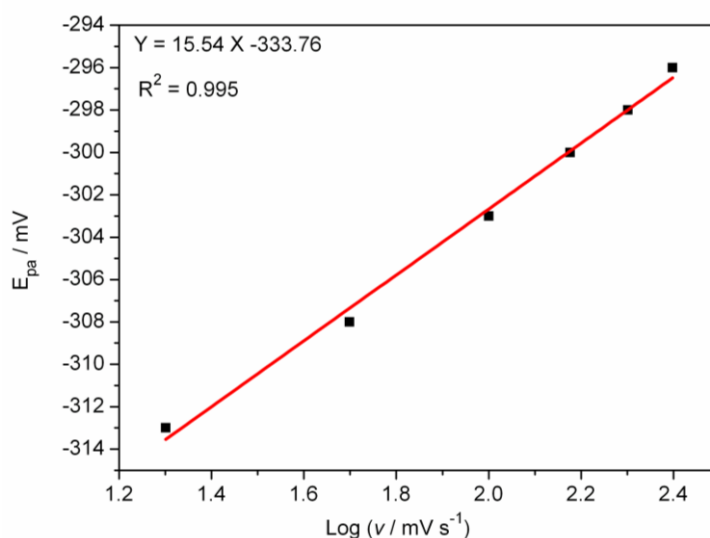

Figure 9. The plot of E_p versus the log of scan rate

IV.   Conclusion

A simple and room-temperature method for the synthesis of PdAuAg nanoclusters has been demonstrated. Fabrication of Pt electrodes by the PdAuAg nanoclusters film provides a promising route for the development of low-cost, high performance electro-catalysts for electro-oxidation of ammonia. The improved catalytic activity of the PdAuAg nanoalloys is attributed to both an increased effective surface area and enhanced electron transfer. Ammonia electro-oxidation on the PdAuAg film modified Pt electrode is controlled by mass-transfer process of ammonia towards the electrode surface.

Acknowledgements

References

[1].   S Dunn, Hydrogen futures: toward a sustainable energy system, *International Journal of Hydrogen Energy, 27*, 2002, 235–264.
[2].   L Arana, S. Schaevitz, A. Franz, M. Schmidt, and K. Jensen, A microfabricated suspended- tube chemical reactor for thermally efficient fuel processing, *Journal of Microelectromechanical Systems, 12*, 2003, 600-612.
[3].   C Zhong, W. Hu, and Y. Cheng, On the essential role of current density in electrocatalytic activity of the electrodeposited platinum for oxidation of ammonia, *Journal of Power Sources, 196*, 2011, 8064-8072.
[4].   S Wasmus, E. Vasini, M. Krausa, H. Mishima, and W. Vielstich, DEMS-cyclic voltammetry investigation of the electrochemistry of nitrogen compounds in 0.5 M potassium hydroxide, *Electrochimica Acta, 39*, 1994, 23-31.
[5].   F Vitse, M. Cooper, and G. Botte, On the use of ammonia electrolysis for hydrogen production, *Journal of Power Sources, 142*, 2005, 18-26.
[6].   L Zhou, and Y. Cheng, Catalytic electrolysis of ammonia on platinum in alkaline solution for hydrogen generation, *International Journal of Hydrogen Energy, 33*, 2008, 5897-5904.
[7].   H Gerischer, and A. Mauerer, Oxidation of Ammonia on an Platinium-Eletrode. *Journal of Electroanalytical Chemistry and Interfacial Electrochemistry*, *25*, 1970, 421-433.
[8].   K Endo, Y. Katayama, and T. Miura, Pt–Ir and Pt–Cu binary alloys as the electrocatalyst for ammonia oxidation, *Electrochimica Acta, 49*, 2004, 1635–1638.
[9].   A Vooys, K. De, R. Santen, and J. Veen, The role of adsorbates in the electrochemical oxidation of ammonia on noble and transition metal electrodes, *Journal of Electroanalytical Chemistry, 506*, 2001, 127-137.
[10].   T. Teranishi and M. Miyake, Size Control of Palladium Nanoparticles and Their Crystal Structures, *Chemistry Materials,10*, 1998, 594

[11]. W Young, H. Naam, Y. Kang, K. Kihyun, K. Minjung, and W. Sang, Synthesis and characterization of flower-shaped porous of Au-Pd Alloy Nanoparticles, *Journal of Physical Chemistry C, 112,* 2008, 6717–6722.

[12]. Y Lee, M. Kim, Y. Kim, S. Kang, J. Lee, and S. Han, Synthesis and Electrocatalytic Activity of Au−Pd Alloy Nanodendrites for Ethanol Oxidation, *The Journal of Physical Chemistry C, 114,* 2010, 7689-7693.

[13]. X Teng, X. Liang, S. Maksimuk, and H. Yang, Synthesis of Porous Platinum Nanoparticles. *Small,* 2, 2006, 249-253.

[14]. J. Hoefelmeyer, K. Niesz, G. Somorjai, and T. Tilley, Radial anisotropic growth of rhodium nanoparticles, *Nano Letters, 5,* 2005, 435-438.

[15]. C Kuo, and M.Huang, Synthesis of branched gold nanocrystals by a seeding growth approach, *Langmuir, 21,* 2005, 2012-2016.

[16]. H Lee, S. Habas, S. Kweskin, D. Butcher, G. Somorjai, and P. Yang, Morphological Control of Catalytically Active Platinum Nanocrystals, *Angewandte Chemie, 118,* 2006, 7988-7992.

[17]. J. Wang, Analytical Electrochemistry. *John Willey and Sons,* Inc, Publication, Newyork 2000, 45-48.

[18]. V Diculescu, A. Chiorcea-Paquim, O. Corduneanu, and A Oliveira-Brett, Palladium nanoparticles and nanowires deposited electrochemically: AFM and electrochemical characterization, *Journal of Solid State Electrochemistry, 11,* 2007, 887-898.

[19]. S Mailu, T. Waryo, P. Ndangili, F. Ngece, A. Baleg, P. Baker, and E. Iwuoha, Determination of Anthracene on Ag-Au Alloy Nanoparticles/Overoxidized-Polypyrrole Composite Modified Glassy Carbon Electrodes, *Sensors, 10,* 2010, 9449-9465.

[20]. T. Liu, T. Kang, L. Lu, Y. Zhang, and S. Cheng, Au-Fe(III) nanoparticle modified glassy carbon electrode for electrochemical nitrite sensor, *Journal of Electroanalytical Chemistry, 632,* 2009, 197-200.

[21]. H. Behzad, H. Hassan, and B. Somayyeh, B. Sensitive and selective determination of hydrazine using glassy carbon electrode modified with Pd nanoparticles decorated multiwalled carbon nanotubes, *Analytical Bioanalytical Chemistry, 398,* 2010, 1411-1416.

[22]. Y. Lee, N. Kim, K. Lee, K. Kwon, M. Kim, and S. Han, Synthesis and Characterization of Flower-Shaped Porous Au−Pd Alloy Nanoparticles, *The Journal of Physical Chemistry C, 112,* 2008, 6717-6722.

[23]. S. Yange, and H. I-Ming, Synthesis of bimetallic PdAu nanoparticles for formic acid oxidation, *Electrochimica Acta, 56,* 2011, 2174-2183.

[24]. T. Katan, and R. Galiotto, Current efficiencies for the anodic oxidation of ammonia in potassium hydroxide solution, *Journal of Electrochemical Society, 110,* 1963, 1022–1023.

[25]. F Vidal-Iglesias, N. Garc-Araez, V. Montiel, J. Feliu, and A. Aldaz, Selective electrocatalysis of ammonia oxidation on Pt(100) sites in alkaline medium, *Electrochemistry Communications, 5,* 2003, 22–26.

[26]. Z Haijiang, H. Jianshe, H. Haoqing, and Y. Tianyan, Electrochemical Detection of Hydrazine Based on Electrospun Palladium Nanoparticle/Carbon Nanofibers, *Electroanalysis, 21,* 2009, 1869–1874.

[27]. H. Yadegari, A Jabbari, H. Heli, A. Moosavi-Movahedi, K. Karimian, and A. Khodadadi, Electrocatalytic oxidation of deferiprone and its determination on a carbon nanotube-modified glassy carbon electrode, *Electrochimica Acta, 53,* 2008, 2907-2916.

[28]. V. Rosca, and M. Koper, Electrocatalytic oxidation of ammonia on Pt(111) and Pt(100) surfaces, *Physical Chemistry Chemical Physics,* 8, 2006, 2513-2524.